To appear in the *Journal of Geophysical Research*, 2001.

ELF/VLF waves correlated with transversely accelerated ions in the auroral region observed by Akebono

Yoshiya Kasahara,[1] Tomohisa Hosoda,[1] Toshifumi Mukai,[2] Shigeto Watanabe,[3] Iwane Kimura,[4] Hirotsugu Kojima,[5] and Ryotaro Niitsu[1]

Abstract

Plasma waves observed by the Akebono satellite in the region of ion heating/acceleration transverse to the geomagnetic field line are studied. Especially, electrostatic, broadband low-frequency noise is closely correlated with transversely accelerated ions. Simultaneous electron precipitation in the energy ranges from a few tens to hundreds eV is also usually observed. Our waveform analysis revealed that the electrostatic broadband noise is classified into two types of noise: one is continuous noise with upper cutoff around a few kilohertz, and the other is an intermittent impulsive waveform extended more than 10 kHz. A possible explanation to the dominant part of continuous broadband noise is that they are ion acoustic waves generated by precipitating electrons (approximately a few hundreds eV) and that the wave is the possible main energy source of ion heating/acceleration. The other mechanisms may, however, be sometimes important for generating the broadband noise. Using long-period observation data sets of Akebono, which is orbiting in the altitude range between 270 and 10,000 km, statistical studies on the spatial and temporal distribution of the continuous broadband noise are made. Several kinds of statistical features are clarified: (1) The occurrence region is distributed in the cusp and along the auroral oval, (2) the region is extended toward the lower latitude while the geomagnetic activity is higher, (3) the intensity is larger in the cusp than it is in the nightside, and (4) it is largest in winter and weakest in summer.

1. Introduction

Ion heating/acceleration transverse to the geomagnetic field line (TAI) in the auroral region is an important phenomenon as it is one of the main causes of ion outflow from the ionosphere to the magnetosphere. A lot of observations of TAI were made by rockets and satellites for more than 20 years [e.g., *Sharp et al.*, 1977; *Whalen et al.*, 1978; *Klumpar*, 1979]. In energizing ions perpendicular to the geomagnetic field line, wave-particle interaction plays an important role. The plasma environment in the auroral region is quite complicated, and the existence of several kinds of plasma wave were reported [e.g., *Gurnett and Frank*, 1978; *Gurnett et al.*, 1984, and references therein]. Many experimental studies on the correlation between TAI and plasma waves such as electrostatic ion cyclotron wave [*Kintner et al.*, 1979, 1989], lower hybrid resonance (LHR) wave [*Vago et al.*, 1992], electrostatic broadband noise [*André et al.*, 1988, 1990], and electromagnetic ion cyclotron wave [*Erlandson et al.*, 1994] were performed. Theoretical studies and computer simulations were also made to clarify the relationship between TAI and these plasma waves, and various heating mechanisms have been proposed [e.g., *Ungstrup et al.*, 1979; *Lysak et al.*, 1980; *Chang and Coppi*, 1981; *Okuda and Ashour-Abdalla*, 1981; *Dusenbery and Lyons*, 1981; *Ashour-Abdalla and Okuda*, 1984; *Chang et al.*, 1986].

The spatial structure in the region of TAI and the correlations between particles and waves were investigated by the recent rocket experiments in detail. SCIFER, which intersected in the cleft ion fountain region at an altitude of $\sim$ 1400 km, observed TAI and closely correlating broadband low-frequency electric fields extended up to a few kilohertz in the latitudinally narrow regions [*Arnoldy et al.*, 1996; *Kintner et al.*, 1996]. AMICIST investigated the nightside auroral ion outflow region at an altitude of $\sim$ 800 km [*Lynch et al.*, 1996; *Bonnell et al.*, 1996]. Two kinds of TAI (one was associated with lower hybrid solitary wave and another was associated with broadband low-frequency electrostatic wave,) were observed, but the most intense TAI was observed where the broadband low-frequency electrostatic wave was enhanced [*Lynch et al.*, 1996].

Observation made by the Freja satellite revealed detailed characteristics of the ion heating and corresponding wave phenomena at an altitude around 1700 km. *Norqvist et al.* [1996] examined particle and wave data and discussed the possible heating mechanisms. They concluded that broadband waves around the ion cyclotron frequencies are the main energy source for the TAI and that the other mechanisms such as lower hybrid wave or slowly varying electric field are less important in the dayside magnetosphere at an altitude around 1700 km. *Wahlund et al.* [1998] investigated the wave phenomena in the region where the ion heating was observed. They suggested that the broadband extremely low frequency wave (BB-ELF) consists of several kinds of wave mode and that the wave in the frequency range between 30 and 400 Hz is dominated by slow ion acoustic waves. *Knudsen et al.* [1998] made correlation analysis of wave and ion data. They introduced the observation examples of ion heating within both regions of VLF hiss and broadband ELF waves. Their analysis showed that correlations are highest for wave frequencies below several hundred hertz and less at VLF hiss frequencies. They also examined the correlation between electron precipitation and ion heating. They found that ion heating is well correlated with precipitating electrons in the energy range below several hundred eV, which are named suprathermal electron bursts (STEB), while the correlation is not so good with the electrons associated with auroral inverted-V's in the energy range above 1 keV. *André et al.* [1998] classified the observation patterns of TAI into four types. They concluded that the common types are the two of them which are both associated with broadband ELF waves. *Norqvist et al.* [1998] studied the parameter dependence of the four types of observation patterns on the magnetic local time, magnetic latitude, magnetic activity, and season. According to their analysis, $\sim$ 90% of oxygen heating events are caused by ion energization associated with broadband low-frequency waves, and the prenoon auroral region is a major source of oxygen ions energized by broadband low-frequency waves.

In the present paper, plasma waves correlated with ion heating and acceleration observed by the Akebono satellite are studied. Akebono covers the wide altitude range between 270 and 10,000 km over all local time in the period of more than 11 years. Using long-period observation data sets obtained by Akebono, the global distribution of plasma waves in the auroral region and observational relationship between particles and waves can be clarified quantitatively. Our aim in the present paper is firstly to examine the characteristics of the plasma waves in the regions of TAI observed by Akebono. We show that broadband low-frequency waves are closely correlated with TAI

in the auroral region, as was suggested by many authors. Secondly, we investigate the average intensity of the broadband low-frequency wave and its temporal and spatial distributions statistically using long-period observation data sets of Akebono. The results are important clues to understanding the TAI and the ion outflow from the ionosphere. Finally, we suggest a possible scenario of the energy transport between waves and particles.

2. Instruments on board the Akebono Satellite

The Akebono (Exos D) satellite was launched in February 1989, with the altitude range from 270 to 10,000 km and an inclination of 75°. The satellite is equipped with several kinds of scientific instruments to investigate the plasma phenomena in the auroral region. Akebono was successfully operated for more than 11 years after launch. The large amount of data obtained by Akebono is suitable for the statistical study in a solar cycle. The scientific instruments used for the present study are briefly described.

The VLF instruments are designed to investigate plasma waves from a few hertz to 17.8 kHz [*Kimura et al.*, 1990; *Hashimoto et al.*, 1997]. The electric components of the plasma wave are taken from two sets of crossed dipole antennas with a tip-to-tip length of 60 m. The magnetic wave fields are sensed by three orthogonal loop antennas and three orthogonal search coils for the frequencies above and below 800 Hz, respectively. The signals detected by the electric and magnetic sensors are processed by the subsystems in the VLF instruments. In the present paper we utilize the data obtained by the following subsystems: (1) the multichannel analyzer (MCA), which measures one component of E and B field at 16 frequency points from 3.18 Hz to 17.8 kHz; (2) the ELF receiver (ELF), which measures waveforms taken by both E and B sensors in the frequency range below 80 Hz in the ELF-narrow mode or 160 Hz in the ELF-wide mode; and (3) the wideband receiver (WBA), which is an analogue receiver for one component of E or B field below 15 kHz.

The low-energy particle detector (LEP) measures energy and pitch angle distributions of electrons from 10 eV to 16 keV and ions from 13 eV to 20 keV [*Mukai et al.*, 1990]. The suprathermal ion mass spectrometer (SMS) measures two-dimensional energy distributions in the satellite spin plane of thermal (0–25 eV) and suprathermal (25 eV to several keV) ion [*Whalen et al.*, 1990; *Watanabe et al.*, 1992].

3. Observations

One example of correlation diagram between wave and particle observed by Akebono on July 11, 1991, is shown in Plate 1. Plates 1a and 1b show electric and magnetic wave spectrum observed by MCA, respectively. It should be noted that the stripes which periodically appear in Plate 1b every $\sim$ 40 s are the noise by interference from other scientific instrument on board the satellite. Plates 1c-1e and Plates 1f-1h show pitch angle sorted energy spectograms of electrons and ions, respectively, observed by LEP. These panels are sorted by pitch angle ranges of 0°–60°, 60°–120°, and 120°–180°. Since the data were obtained by energy per charge analyzers, ion compositions in the ion energy spectograms are unknown. The following parameters stand for universal time (UT), altitude (ALT), magnetic local time (MLT), magnetic latitude (MLAT), invariant latitude (ILAT), and L value along the trajectory of Akebono. As Akebono is orbiting from 4500 to 7500 km in ALT in the Northern Hemisphere, the pitch angles of 0° and 180° correspond to the downward and upward directions, respectively, along the geomagnetic field line in this case.

In the spectograms for ions in Plate 1, ion precipitation in the energy range from 10 keV down to several hundreds eV are recognized from 0537:00 to 0547:50 UT. It indicates that Akebono is skimming along the cusp region. The precipitating ion flux is enhanced from 0537:30 to 0541:20 UT, from 0545:20 to 0546:00 UT, and from 0547:20 to 0547:50 UT, and the wave from 400 Hz to $\sim$ 3 kHz is simultaneously observed both in electric and magnetic components. As a result of the detailed investigation using the analogue data obtained by WBA, we find that the wave exists harmonically just above the local cyclotron frequency of H^+ and its harmonics. This wave is therefore supposed to be an electromagnetic ion cyclotron harmonic (ICH) wave generated by the precipitating ions, but we do not discuss this further, because this is not the main subject of the present paper.

In the panels of ion spectograms for the pitch angle ranges of 60°–120° and 120°–180° (Plates 1g and 1h), TAI and ion conics are observed in the energy range below a few hundreds eV during the following three periods: from 0537:30 to 0541:50 UT, from 0542:20 to 0546:10 UT, and from 0547:20 to 0547:50 UT. Although there are several kinds of waves in the region where the TAI and ion conics are observed, broad-

band noise in the frequency range from a few kilohertz down to a few hertz looks well correlated with them; that is, the noise is detected from 0537:10 to 0541:50 UT, from 0542:00 to 0547:00 UT, and from 0547:20 to 0547:50 UT. There is another significant wave, which is a hiss-like emission in the frequency range from a few kilohertz up to more than 10 kHz, but this wave does not always correspond with the changes of ion flux.

The broadband noise has a magnetic component below 20 Hz although the upper cutoff of the magnetic component is not clear because of the interference. Thus this frequency part shows an Alfvénic feature as was suggested by many authors based on the observation from Fast Auroral Snapshot Explorer (FAST) and Freja satellites [e.g., *Seyler et al.*, 1995; *Wahlund et al.*, 1998; *Chaston et al.*, 1999; *Stasiewicz et al.*, 2000, and references therein]. In the higher frequency range the broadband noise becomes electrostatic. The upper cutoff of the electric component of the broadband noise is $\sim$ 200 Hz in the periods of 0537:10–0541:50 and 0547:20–0547:50 UT, but it increases up to $\sim$ 1 kHz in the period of 0542:00–0547:00 UT, when the total flux of heated ions becomes largest. Additionally, it is noted that electron precipitation in the energy range below a few hundreds eV down to a several tens eV is simultaneously observed in the spectograms for electrons in Plate 1, although the detailed feature of the electron flux does not exactly correspond with those of heated ions and broadband noise.

The data obtained by SMS are useful for the identification of the initial stage of TAI and the investigation of the relationship between TAI and broadband noise, because SMS covers a lower energy range than LEP does. Plate 2 shows the summary plot of thermal and suprathermal ions simultaneously observed by SMS. In Plate 2, two-dimensional energy and spin angle distributions for four kinds of thermal ions (H^+, He^+, O^+, and O^{++}) are shown in Plates 2a-2d. V and r in Plate 2e show the energy steps (solid lines) and the angle of closest approach of the SMS field of view to the ram direction (a dashed line), respectively. The scales are displayed on the left (eV) and right (degree) axes, respectively. In the same way, two-dimensional energy and spin angle distributions for two major suprathermal ions (H^+ and O^+) are shown in Plates 2f and 2g. E and p in Plate 2h show the suprathermal energy steps (solid lines) and the minimum pitch angle sampled during one spin (a dashed line), respectively. The scales are also displayed on the left (eV) and right (degree) axes, respectively. Zero degree of the spin angle corresponds to the minimum pitch angle in the spin plane of the Akebono satellite. The dashed lines around 40° in Plates 2a-2d and Plates 2f-2g show the spin angle closest to the ram direction in the spin plane. We see that all kinds of thermal ions are transversely accelerated and going upward as ion conics in the periods of 0537:40–0541:20, 0542:40–0547:00, and 0547:30–0547:50 UT. Although we must notice that the region of ion conics is possibly affected by convection, the observational result shows that the regions of TAI and ion conics are generally identical with the regions where the broadband noises are observed.

According to the observation by Akebono, this kind of correlation is commonly observed in the cusp and along the auroral oval. The energy densities of the ion heating and ion conics are relatively higher in the dayside, especially in the cusp, than in the nightside region. We discuss this point later in relation to the statistical results described in section 5.

As was mentioned in section 2, our wideband receiver named WBA covers the frequency range below 15 kHz, and the obtained data are sent by analogue telemetry. In order to investigate the characteristics of the broadband noise in detail, we analyzed the spectrum and its waveform of the broadband noise with a high time resolution using the data obtained by WBA. WBA was measuring the electric wave field on July 11, 1991.

The upper panel in Plate 3 shows an enlarged dynamic spectra of an electric field which is made from the WBA data by fast Fourier transform (FFT) analysis. The electric wave field from 0542:40 to 0543:20 UT on July 11, 1991, is shown. The in situ plasma frequency and cyclotron frequency of electrons are 220.3 and 161.1 kHz, respectively. These frequencies are derived from the local UHR frequency measured by Plasma Wave and Sounder (PWS) on board Akebono (H. Oya et al., private communication, 1998) and the International Geomagnetic Reference Field (IGRF) magnetic field model. Hence the local LHR frequency and proton cyclotron frequency are 3.0 kHz and 120 Hz, respectively. A sharp cutoff above 15 kHz in the upper panel is due to the low-pass characteristics of WBA, and the stripes which periodically appear from 0 to 20 kHz are caused by interference from other instruments. In the upper panel a hiss-like emission which has a lower cutoff above the local LHR frequency is observed.

As for the broadband noise in the lower frequency

range, we can distinguish two types of noise as described in the following. One is a low-frequency noise continuously observed below 1 kHz. The other is impulsive noise which occurs intermittently with a short duration, and its spectrum is extended up to 10 kHz. The lower panel in Plate 3 shows the angles between the wire antenna and the geomagnetic field line. It is found that the upper cutoff frequency of the continuous type of broadband noise decreases when the antenna angle approaches perpendicular to the geomagnetic field line. This fact suggests that the electric wave field of the noise is oscillating nearly in the parallel direction of the geomagnetic field line. The intermittent type of broadband noise also tends to have a similar spin dependence, but it is not so clearly distinguished, owing to a poor signal-to-noise (S/N) condition.

The waveforms of both broadband noises are analyzed. In the analysis the WBA analogue data were sampled with a sampling frequency of 51.2 kHz. Figure 1 indicates the waveform from 0542:44.929 UT with a time interval of 320 ms when the impulsive type of broadband noise is observed. We find that solitary structures are observed as a series of pulses. The amplitude of each pulse is about a few mV m^{-1} peak to peak, and the pulse width is usually less than 1 ms. It should be mentioned that the waveform is very similar to those observed in the auroral region by FAST [*Ergun et al.*, 1998] and Polar [*Franz et al.*, 1998] and in the Earth's magnetotail by Geotail [*Matsumoto et al.*, 1994; *Kojima et al.*, 1997]. This impulsive noise may reflect the small-scale potential structure, and it is assumed to be an electrostatic solitary wave (ESW), introduced by *Matsumoto et al.* [1994]. So far, as we examined waveforms for other trajectories, it is found that this type of solitary waveform was usually recognized in the duskside auroral region in the altitude above 2500 km but not so often recognized in the other region. As we have not yet examined many trajectories, more detailed characteristics of the intermittent noise will be reported in a subsequent paper.

On the other hand, the waveform of the continuous broadband noise below 1 kHz does not include a solitary structure and is quite randomly oscillating (not shown here). This kind of continuous random noise is almost always observed in the cusp and auroral oval region, and its upper cutoff exists ordinarily around a few kilohertz.

We summarize our observations as follows. We observe several kinds of plasma wave in the ion heating/acceleration region: hiss or LHR noise, ion cyclotron harmonic wave, and two types of broadband noise. We find that the continuous type of broadband noise in the frequency range below a few kilohertz is ordinarily observed in the auroral region and is most correlated with ion heating/acceleration and ion conics, so that this wave is the possible main energy source of ion heating/acceleration. This noise is electrostatic in the higher frequency range, but it becomes electromagnetic and shows Alfvén-like characteristics in the lower frequency range generally below the local oxygen cyclotron frequency. In the region where this type of broadband noise is observed, precipitating electrons in the energy range below a few hundreds eV are usually observed. We should also note that wave intensities of the broadband emissions detected by dipole antennas with a tip-to-tip length of 60 m on board Akebono tend to be estimated smaller than the real ones, since the wavelength of the broadband emissions must be quite short especially in the higher frequency range. In the present paper, however, we use the detected wave intensity as we mainly discuss the features of broadband noise below 80 Hz, where the effect of attenuation may not be so large.

4. Correlation Between Plasma Wave and Particle Data

In this section, we discuss the interrelationship between continuous broadband noises and particles in detail. In order to investigate the interaction process between wave and particle, we examined the correlation between the energy densities of broadband noise and heated ion. In the analysis we selected typical cases of 22 trajectories in which TAI and ion conics were recognized by LEP. In other words, these are the cases in which ions were sufficiently heated in the energy range of ~100 eV. We should also note that these typical cases were all observed at the altitude above 3000 km. We calculate the velocity distribution function of ions using the data obtained by LEP, and we estimated the energy density of TAI in the energy range below 340 eV assuming that ions are all protons. As for the electric intensity of the broadband noise, we calculate spectral density in the frequency range below 10 Hz using the data from the ELF subsystem. Figure 2 is a scatterplot which indicates the relationship between spectral density of the broadband noise and energy density of heated ions in every 32 s. The circles and pluses mean that the data were obtained in the dayside and in the nightside, respectively.

We find a clear relationship between wave spectral density and ion energy density in Figure 2. It is also found that wave spectral density is generally larger in the dayside than in the nightside, and the corresponding ion energy density has a similar tendency. An important point to be noted is that there is a threshold level in the wave spectral density, and ions can be efficiently energized when the wave spectral density is larger than the threshold level. In other words, there are some cases in which ion energy density is small and wave spectral density is rather large, while the opposite case is rarely found. This fact shows that an intense wave is needed for ions to be highly energized. Therefore it is suggested that the broadband noise is the energy source of the ion heating/acceleration, and some other energy source should be taken into account for the generation of the broadband noise. This tendency is also reported by *Knudsen et al.* [1998], and our result shows a good agreement with them even though the data used in the present study are obtained at the altitude above 3000 km.

5. Statistical Study

Akebono was launched in February 1989 and was successfully operated for more than 11 years. The large amount of obtained data is quite valuable for the statistical study on the spatial and temporal distribution of various kinds of wave and particle phenomena as a function of multidimensional parameters of local time, season, solar activity, geomagnetic activity, etc. In this section, statistical characteristics on the continuous broadband noise using the data sets obtained by Akebono are reported.

We made the statistical studies using the data taken from the ELF subsystem. We first calculate the average intensity of the electric wave field below 80 Hz with a frequency resolution of 2.5 Hz every 8 s by FFT. In the present statistical study, the data processing was carried out for the data obtained from February 1989 until the end of 1998.

The data coverage of Akebono used for the study is shown in Figure 3. The total number of the satellite paths was $\sim$ 27,000. The left panel shows the total number of data points projected on the geomagnetic meridian plane at all magnetic local times. The solid curves in the panel are the geomagnetic field lines of the dipole model, and R_E is the radius of the Earth. We divide the panel into 200 grids along the vertical axis and 100 grids along the horizontal axis, and we indicate the number of data points at each pixel surrounded by the grids using the tone pattern shown in the right corner. The upper and lower panels on the right side show the number of data points when Akebono is located in the Northern and Southern Hemispheres, respectively. In these panels, invariant latitude (ILAT) is shown by the radius of the circle, and magnetic local time is taken along the circumference. The number of data points with less than 60° ILAT is not shown in the panels. We divide each panel into 100 by 100 grids vertically and horizontally, and we show the number of data points accumulated along the entire altitude range at each pixel by the same tone pattern used for the left panel.

As shown in Figure 3, the data coverage is coarse in the equatorial region but quite fine in the polar region because the data acquisition of Akebono is mainly made from ground stations located at high-latitude areas in Canada, Sweden, and Antarctica. In the present study, we concentrate on the region larger than 60° ILAT, where the number of data points at each pixel is at least 100. In the following we average the intensity of the electric wave field at each pixel and discuss the spatial and temporal distribution of the continuous broadband noise.

Plate 4 shows the average intensity of the electric wave field at 5 Hz. In Plate 4, the contour level indicates the average electric intensity as shown by the color code in the right corner. The region below 60° ILAT is excluded in the left panel. As the continuous broadband noise is observed almost every time when Akebono traverses the polar region and as its intensity is generally the largest among plasma waves in the polar region at 5 Hz, Plate 4 reflects the spatial distribution of the continuous broadband noise.

In the left panel the broadband noise is observed along the geomagnetic field line from 65° to 80° ILAT. In the right two panels the broadband noise is distributed at all local times. These facts support the observation result that the continuous broadband noise is usually observed in the cusp and auroral oval region regardless of the local time and the altitude. The most intense broadband noise with an average intensity of 0.3–0.5 mV $m^{-1}/\sqrt{Hz}$ is located between 75° and 80° ILAT around noon, which corresponds with the cusp region. The active region shifts toward the lower invariant latitude region along the auroral oval as the magnetic local time approaches midnight, and finally the region is located between 65° and 72° ILAT around midnight. The lowest average intensity is $\sim$ 0.2 mV $m^{-1}/\sqrt{Hz}$ in the magnetic local time range from 17 to 22.

The other frequency points below 80 Hz are also examined. It is consequently found that the active region is almost the same, although the intensity becomes smaller for the higher frequency point. As the frequency range of the ELF subsystem is quite low compared to the upper cutoff of the continuous broadband noise which generally exists around a few kilohertz, we do not discuss the statistical characteristics of the upper cutoff of the noise in the present paper. The data obtained by MCA are useful for detecting the upper cutoff of the noise, but it is difficult to distinguish the continuous broadband noise automatically from the other plasma waves in the kilohertz range. We should also note that the frequency range below 80 Hz is the rather Alfvénic part of the emission, and thus the distribution region of the emissions at a higher frequency range might be different from those of the Alfvénic part. We leave those problems, however, to future work and focus on the results derived from the intensity map of the electric field at 5 Hz in this paper.

Plates 5a-5c indicate the average intensity of the electric wave field at 5 Hz at 0000–0800, 0800–1600, and 1600–0000 MLT, respectively. The intensity is shown by the same color code used in Plate 4. The most active region is distributed around the noon along the all altitude region from 10,000 km down to a few hundreds of kilometers in quite a narrow invariant latitude range centered at 78° as shown in Plate 5b. The average intensity in this region is 0.3–0.5 mV $m^{-1}/\sqrt{Hz}$ in general.

In the postmidnight and dawn sectors (Plate 5a), the active region is mainly distributed in the broad invariant latitude range between 65° and 80° in the altitude region higher than 3000 km. The active regions in the dusk and premidnight sectors (Plate 5c) are similar to those in the postmidnight and dawn sectors, but the intensity is comparatively weak.

The distribution of the continuous broadband noise as a function of Kp index is shown in Plate 6. The intensity is shown by the same color code used in Plate 4. Plates 6a-6c show the average intensity of the broadband noise at 5 Hz at $Kp \leq 2+$, $3- \leq Kp \leq 4+$, and $5- \leq Kp$, respectively. The broadband noise is observed to be stationary even though the geomagnetic activity is quiet and the region is distributed in the higher latitude side. As the geomagnetic activity becomes higher, the occurrence region is extended toward the lower latitude side and scattered in the broad latitude range. The average intensity at higher Kp index becomes apparently small, but this may be explained by the following reason. The spatial structure is quite stable when the geomagnetic activity is quiet. On the contrary, the structure dynamically changes by the geomagnetic condition at higher Kp, and it consequently causes the relatively small intensity on average.

The seasonal variation of the intensity and occurrence region of the noise at 5 Hz is also examined. One year is divided into four seasons whose center is chosen at equinoxes and solstices as follows: (1) February 7 to May 6, (2) May 7 to August 6, (3) August 7 to November 6, and (4) November 7 to February 6. The average intensity of the electric field at 5 Hz for each season is shown in Plate 7 by the same color code as that used in Plate 4. Plates 7a-7d show the contour maps in the Northern Hemisphere, and Plates 7e-7h show those in the Southern Hemisphere. It is very interesting that the wave activity becomes highest in the winter hemisphere and lowest in the summer hemisphere. In the summer hemisphere the intensity is quite weak, and the main active region, where the average intensity is larger than 0.3 mV $m^{-1}/\sqrt{Hz}$, is limited around the cusp region. On the other hand, in the winter hemisphere the active region becomes wider in invariant latitude and is extended along the auroral oval, especially toward the dawn and postmidnight sectors. The average intensity also increases up to 0.5 mV $m^{-1}/\sqrt{Hz}$ except in the region of 1500–2100 MLT.

6. Discussions and Conclusions

In the present paper we studied plasma waves correlated with ion heating and acceleration observed by the Akebono satellite. We firstly investigated the correlation between waves and particles in the region of TAI and ion conics, and we showed that broadband noise is commonly observed in the region. Our waveform analyses clarified that broadband electrostatic noise consists of two kinds of wave. One is intermittent impulsive wave in the frequency range up to 10 kHz, and the other is continuous random noise below a few kilohertz. We demonstrated that the continuous type of broadband noise is closely correlated with TAI and ion conics and that this wave is the possible main energy source of ion heating/acceleration transverse to the geomagnetic field line.

Our statistical study showed that the continuous type of electrostatic broadband noise is observed at all local times in the auroral region. In the cusp region the intensity is highest, and it is almost constant along

the magnetic field lines at the entire altitude range of Akebono, which is from 270 to 10,000 km. Outside the cusp the broadband noise is also distributed along the magnetic field line, but the intensity becomes smaller at altitudes below 3000 km. Moreover, the intensity of the broadband noise becomes less in the dusk and premidnight sectors.

A similar statistical study was made by *Gurnett and Frank* [1977] using the data from Hawkeye 1 and Imp 6. They analyzed occurrence frequency of the broadband electrostatic noise as a function of magnetic latitude and magnetic local time in the region from 5.01 to 6.31 R_E. They concluded that the broadband noise occurs at all local times. Our observation was made in the lower altitude region, so that the continuous broadband noise is possibly distributed at all altitude regions below several R_E along the auroral field lines. However, we should note that the broadband electrostatic noise observed by Hawkeye 1 and Imp 6 is much more intense in the nightside than in the cusp [*Gurnett and Frank*, 1978] in contrast to our result. This may be because the altitude range of Akebono is lower than those of Hawkeye 1 and Imp 6.

When these statistical results are compared to those for ion outflow phenomena, a clear relationship can be found between broadband noise and TAI. As we mentioned in section 3, we found that TAIs and ion conics recognized by the SMS instruments occur in the exact timing of the broadband noise enhancement for most data sets obtained by Akebono. Furthermore, the region of ion outflow, which is statistically analyzed using the data from SMS, is quite similar to the region of broadband noise (S. Watanabe et al., private communication, 1999).

In the altitude region from 8000 to 23,300 km, *Yau et al.* [1984] reported that the occurrence frequency distribution of upflowing ionospheric ion (UFI) observed by DE 1 is "auroral-oval-like"; namely, the frequency peaks at a more equatorward latitude and has a broader latitudinal extent in the nightside than in the dayside. An extended study of *Yau et al.* [1984] was made by *Kondo et al.* [1990]. *Kondo et al.* [1990] made a statistical analysis of upflowing ion beam and conic distributions at DE 1 altitude and found that upflowing beams tended to occur between dusk and premidnight, while conics were observed mostly between dawn and noon. Our statistical results show that continuous broadband noise is intense between dawn and noon and weak in the dusk region; therefore these results show a good agreement with the mechanism that ions are energized by continuous broadband noise and going upward as ion conics.

On the other hand, patterns of TAI observed by Freja at the altitude around 1700 km were classified into four types [*André et al.*, 1998], and it is suggested that $\sim 90\%$ of oxygen heating events are caused by ion energization associated with broadband low-frequency waves [*Norqvist et al.*, 1998]. *André et al.* [1998] showed that the TAIs associated with broadband noise are mainly observed in the prenoon auroral sector, and lower hybrid wave or electromagnetic ion cyclotron waves are dominant in the eveningside. The altitude of 1700 km is comparable to or lower than that of Akebono, and our result is also consistent with the results by *André et al.* [1998] from the other point of view that the intensity of the broadband noise is the lowest in the altitude below 3000 km in the dusk and premidnight sectors as was shown in Plate 5 and that other types of ion energization mechanism should be dominant in the region. As for the Kp dependence of the broadband noise, the distributions as a function of Kp indicated in Plate 6 also show a general agreement with the Kp or AE dependence of the ion outflow region [*Norqvist et al.*, 1998; *Øieroset et al.*, 1999].

We also found an interesting feature on the seasonal variation of the broadband noise intensity: The activity of the broadband noise is limited around the cusp region in summer, while it becomes highest in winter and the region extends toward the dawn and postmidnight sectors. Similar seasonal variations are found in electron precipitation [*Newell et al.*, 1996]. *Newell et al.* [1996] reported that the injected electrons are enhanced in winter and suppressed in summer, controlled by the ionospheric conductivity. Although their interpretation can be mainly applicable to the electrons which cause discrete aurora, the same mechanism may work on the generation of the broadband noise. Furthermore, we point out other effects in the generation of broadband noise. As electron density in the ionosphere decreases in winter, density gradient and ratio of precipitating electrons to background electrons also affect the growth rate of broadband noise. As for the seasonal variation of the TAI, *Norqvist et al.* [1998] also pointed out that the occurrence frequency of the ion heating at the Freja altitude is highest in winter while an opposite relationship was found at the higher altitude region of DE 1 [*Yau et al.*, 1985]. We also checked seasonal variation of broadband noise using just data from high altitudes above 6000 km in order to see if the sea-

sonal variation shows agreement with that of *Yau et al.* [1985]. The results are, however, almost the same as those in Plate 7. This may be because the apogee of Akebono is at most 10,300 km, which is much lower than that of DE 1.

Finally, we discuss a possible scenario of the energy transport between waves and particles. According to the numerical calculation for linear dispersion of plasma waves, ion acoustic waves can be generated in the broad frequency range below a few kilohertz by precipitating electrons in the energy range of a few hundreds eV; hence the dominant part of continuous broadband noise possibly consists of ion acoustic waves. The spin dependence of the continuous broadband noise shown in Plate 3 is also consistent with this result. However, there still remains another problem to be solved. According to the results by *Wahlund et al.* [1998], the bulk thermal ion population might be very hot, which makes it hard to grow ion acoustic waves. Furthermore, as the electric component of ion acoustic waves essentially oscillates almost along the geomagnetic field line, efficiency of energy conversion from wave to TAI would not be so high. The plasma environment in the region of TAI is quite complicated, and further consideration such as nonlinear effects may be needed, as was discussed by *Seyler et al.* [1998], *Gavrishchaka et al.* [1999], and other authors. The Akebono data collected over more than 11 years is quite valuable for further investigation, and a more detailed comparison study between wave and particle data will provide a clue to solving this problem in the future.

Acknowledgments. We are grateful to I. Nagano and the other Akebono/VLF members for their support. The authors would like to thank Y. Omura and H. Matsumoto for their helpful comments and suggestions throughout the present work. We also thank T. Nakano for developing analysis software for statistical study. Kp index was referred to a database archived at WDC for geomagnetism, Kyoto. We would like to thank the ISAS Akebono mission project team and the members of the tracking stations at Kagoshima Space Center, Syowa Base in Antarctica, Prince Albert in Canada, and Esrange in Sweden. This research has been financially supported through a grant-in-aid for scientific research from the Ministry of Education, Science, Sports and Culture of Japan (grants 10440138 and 10143102).

Janet G. Luhmann thanks Patrik Norqvist and Jan-Erik Wahlund for their assistance in evaluating this paper.

References

André, M., H. Koskinen, L. Matson, and R. Erlandson, Local transverse ion energization in and near the polar cusp, *Geophys. Res. Lett.*, *15*, 107-110, 1988.

André, M., G. B. Crew, W. K. Peterson, A. M. Persoon, C. J. Pollock, and M. J. Engebretson, Ion heating by broadband low-frequency waves in the cusp/cleft, *J. Geophys. Res.*, *95*, 20,809-20,823, 1990.

André, M., P. Norqvist, L. Andersson, L. Eliasson, A. I. Eriksson, L. Blomberg, R. E. Erlandson, and J. Waldemark, Ion energization mechanisms at 1700 km in the auroral region, *J. Geophys. Res.*, *103*, 4199-4222, 1998.

Arnoldy, R. L., K. A. Lynch, P. M. Kintner, J. Bonnell, T. E. Moore, and C. J. Pollock, SCIFER: Structure of the cleft ion fountain at 1400 km altitude, *Geophys. Res. Lett.*, *23*, 1869-1872, 1996.

Ashour-Abdalla, M., and H. Okuda, Turbulent heating of heavy ions on auroral field lines, *J. Geophys. Res.*, *89*, 2235-2250, 1984.

Bonnell, J., P. Kintner, J.-E. Wahlund, K. Lynch, and R. Arnoldy, Interferometric determination of broadband ELF wave phase velocity within a region of transverse auroral ion acceleration, *Geophys. Res. Lett.*, *23*, 3297-3300, 1996.

Chang, T., and B. Coppi, Lower hybrid acceleration and ion evolution in the suprauroral region, *Geophys. Res. Lett.*, *8*, 1253-1256, 1981.

Chang, T., G. B. Crew, N. Hershkowitz, J. R. Jasperse, J. M. Retterer, and J. D. Winningham, Transverse acceleration of oxygen ions by electromagnetic ion cyclotron resonance with broad band left-hand polarized waves, *Geophys. Res. Lett.*, *13*, 636-639, 1986.

Chaston, C. C., C. W. Carlson, W. J. Peria, R. E. Ergun, and J. P. MacFadden, FAST observations of inertial Alfven waves in the dayside aurora, *Geophys. Res. Lett.*, *26*, 647-650, 1999.

Dusenbery, P. B., and L. R. Lyons, Generation of ion-conic distribution by upgoing ionospheric electrons, *J. Geophys. Res.*, *86*, 7627-7638, 1981.

Ergun, R. E., et al., FAST satellite observations of large-amplitude solitary structures, *Geophys. Res. Lett.*, *25*, 2041-2044, 1998.

Erlandson, R. E., L. J. Zanetti, M. H. Acuña, A. I. Eriksson, L. Eliasson, M. H. Boehm, and L. G. Blomberg, Freja observations of electromagnetic ion cyclotron ELF waves and transverse oxygen ion acceleration on auroral field lines, *Geophys. Res. Lett.*, *21*, 1855-1858, 1994.

Franz, J. R., P. M. Kintner, and J. S. Pickett, Polar observations of coherent electric field structures, *Geophys. Res. Lett.*, *25*, 1277-1280, 1998.

Gavrishchaka, V. V., S. B. Ganguli, and G. I. Ganguli, Electrostatic oscillations due to filamentary structures

in the magnetic-field-aligned flow: The ion-acoustic branch, *J. Geophys. Res.*, *104*, 12,683-12,693, 1999.

Gurnett, D. A., and L. A. Frank, A region of intense plasma wave turbulence on auroral field lines, *J. Geophys. Res.*, *82*, 1031-1050, 1977.

Gurnett, D. A., and L. A. Frank, Plasma waves in the polar cusp: Observations from Hawkeye 1, *J. Geophys. Res.*, *83*, 1447-1462, 1978.

Gurnett, D. A., R. L. Huff, J. D. Menietti, J. L. Burch, J. D. Winningham, and S. D. Shawhan, Correlated low-frequency electric and magnetic noise along the auroral field lines, *J. Geophys. Res.*, *89*, 8971-8985, 1984.

Hashimoto, K., I. Nagano, M. Yamamoto, T. Okada, I. Kimura, H. Matsumoto, and H. Oki, Exos-D (Akebono) very low frequency plasma wave instruments (VLF), *IEEE Trans. Geoelectr. Remote Sens.*, *35*, 278-286, 1997.

Kimura, I., K. Hashimoto, I. Nagano, T. Okada, M. Yamamoto, T. Yoshino, H. Matsumoto, M. Ejiri, and K. Hayashi, VLF observations by the Akebono (Exos–D) satellite, *J. Geomagn. Geoelectr.*, *42*, 459-478, 1990.

Kintner, P. M., M. C. Kelley, R. D. Sharp, A. G. Ghielmetti, M. Temerin, C. Cattell, P. F. Mizera, and J. F. Fennell, Simultaneous observations of energetic (keV) upstreaming and electrostatic hydrogen cyclotron waves, *J. Geophys. Res.*, *84*, 7201-7212, 1979.

Kintner, P. M., W. Scales, J. Vago, R. Arnoldy, G. Garbe, and T. Moore, Simultaneous observations of electrostatic oxygen cyclotron waves and ion conics, *Geophys. Res. Lett.*, *16*, 739-742, 1989.

Kintner, P. M., J. Bonnell, R. Arnoldy, K. Lynch, C. Pollock, and T. Moore, SCIFER: Transverse ion acceleration and plasma waves, *Geophys. Res. Lett.*, *23*, 1873-1876, 1996.

Klumpar, D. M., Transversely accelerated ions: An ionospheric source of hot magnetospheric ions, *J. Geophys. Res.*, *84*, 4229-4237, 1979.

Knudsen, D. J., J. H. Clemmons, and J.-E. Wahlund, Correlation between core ion energization, suprathermal electron bursts, and broadband ELF plasma waves, *J. Geophys. Res.*, *103*, 4171-4186, 1998.

Kojima, H., H. Matsumoto, S. Chikuba, S. Horiyama, M. Ashour-Abdalla, and R. R. Anderson, Geotail waveform observations of broadband/narrowband electrostatic noise in the distant tail, *J. Geophys. Res.*, *102*, 14,439-14,455, 1997.

Kondo, T., B. A. Whalen, A. W. Yau, and W. K. Peterson, Statistical analysis of upflowing ion beam and conic distributions at DE 1 altitudes, *J. Geophys. Res.*, *95*, 12,091-12,102, 1990.

Lynch, K. A., R. L. Arnoldy, P. M. Kintner, and J. Bonnell, The AMICIST auroral sounding rocket: A comparison of transverse ion acceleration mechanisms, *Geophys. Res. Lett.*, *23*, 3293-3296, 1996.

Lysak, R. L., M. K. Hudson, and M. Temerin, Ion heating by strong electrostatic ion cyclotron turbulence, *J. Geophys. Res.*, *85*, 678-686, 1980.

Matsumoto, H., H. Kojima, T. Miyatake, Y. Omura, M. Okada, I. Nagano, and M. Tsutsui, Electrostatic solitary waves (ESW) in the magnetotail: BEN wave forms observed by Geotail, *Geophys. Res. Lett.*, *21*, 2915-2918, 1994.

Mukai, T., et al., Low energy charged particle observations in the "auroral" magnetosphere: First results from the Akebono (Exos-D) satellite, *J. Geomagn. Geoelectr.*, *42*, 479-496, 1990.

Newell, P. T., C.-I. Meng, and K. M. Lyons, Suppression of discrete aurorae by sunlight, *Nature*, *381*, 766-767, 1996.

Norqvist, P., M. André, L. Eliasson, A. I. Eriksson, L. Blomberg, H. Lühr, and J. H. Clemmons, Ion cyclotron heating in the dayside magnetosphere, *J. Geophys. Res.*, *101*, 13,179-13,193, 1996.

Norqvist, P., M. André, and M. Tyrland, A statistical study of ion energization mechanisms in the auroral region, *J. Geophys. Res.*, *103*, 23,459-23,473, 1998.

Øieroset, M., M. Yamauchi, L. Liszka, S. P. Christon, and B. Hultqvist, A statistical study of ion beams and conics from the dayside ionosphere during different phases of a substorm, *J. Geophys. Res.*, *104*, 6987-6998, 1999.

Okuda, H., and M. Ashour-Abdalla, Formation of a conical distribution and intense ion heating in the presence of hydrogen cyclotron waves, *Geophys. Res. Lett.*, *8*, 811-814, 1981.

Seyler, C. E., J.-E. Wahlund, and B. Holback, Theory and simulation of low-frequency plasma waves and comparison to Freja satellite observations, *J. Geophys. Res.*, *100*, 21,453-21,472, 1995.

Seyler, C. E., A. E. Clark, J. Bonnell, and J.-E. Wahlund, Electrostatic broadband ELF wave emission by Alfvén wave breaking, *J. Geophys. Res.*, *103*, 7027-7041, 1998.

Sharp, R. D., R. G. Johnson, and E. G. Shelly, Observation of an ionospheric acceleration mechanism producing energetic (keV) ions primarily normal to the geomagnetic field direction, *J. Geophys. Res.*, *82*, 3324-3328, 1977.

Stasiewicz, K., Y. Khotyaintsev, M. Berthomier, and J.-E. Wahlund, Identification of widespread turbulence of dispersive Alfvén waves, *Geophys. Res. Lett.*, *27*, 173-176, 2000.

Ungstrup, E., D. M. Klumpar, and W. J. Heikkila, Heating of ions to superthermal energies in the topside ionosphere by electrostatic ion cyclotron waves, *J. Geophys. Res.*, *84*, 4289-4296, 1979.

Vago, J. L., P. M. Kintner, S. W. Chesney, R. L. Arnoldy, K. A. Lynch, T. E. Moore, and C. J. Pollock, Transverse ion acceleration by localized lower hybrid waves in the topside auroral ionosphere, *J. Geophys. Res.*, *97*, 16,935-16,957, 1992.

Wahlund, J.-E., et al., Broadband ELF plasma emission during auroral energization, 1., Slow ion acoustic waves, *J. Geophys. Res.*, *103*, 4343-4375, 1998.

Watanabe, S., B. A. Whalen, and A. W. Yau, Thermal ion observations of depletion and refilling in the plasmaspheric trough, *J. Geophys. Res.*, *97*, 1081-1096, 1992.

Whalen, B. A., W. Bernstein, and P. W. Daly, Low altitude acceleration of ionospheric ions, *Geophys. Res. Lett.*, *5*, 55-58, 1978.

Whalen, B. A., J. R. Burrows, A. W. Yau, E. E. Budzinski, A. M. Pilon, I. Iwamoto, K. Marubashi, S. Watanabe, H. Mori, and E. Sagawa, The suprathermal ion mass spectrometer (SMS) onboard the Akebono (Exos-D) satellite, *J. Geomagn. Geoelectr.*, *42*, 511-536, 1990.

Yau, A. W., B. A. Whalen, W. K. Peterson, and E. G. Shelley, Distribution of upflowing ionospheric ions in the high-altitude polar cap and auroral ionosphere, *J. Geophys. Res.*, *89*, 5507-5522, 1984.

Yau, A. W., P. H. Beckwith, W. K. Peterson, and E. G. Shelley, Long-term (solar cycle) and seasonal variations of upflowing ionospheric ion events at DE 1 altitudes, *J. Geophys. Res.*, *90*, 6395-6407, 1985.

T. Hosoda, Y. Kasahara, and R. Niitsu, Dept. of Communications and Computer Eng., Kyoto University, Sakyo-ku, Kyoto 606-8501, Japan. (kasahara@kuee.kyoto-u.ac.jp)

I. Kimura, Dept. of Information System, Osaka Institute of Technology, Hirakata 573-0196, Japan.

H. Kojima, Radio Science Center for Space and Atmosphere, Kyoto University, Uji 611-0011, Japan.

T. Mukai, Institute of Space and Astronautical Science, Sagamihara 229-0022, Japan.

S. Watanabe, Dept. of Science, Hokkaido University, Sapporo 060-0810, Japan.

Received August 18, 2000; revised December 11, 2000; accepted January 8, 2001.

[1]Department of Communications and Computer Engineering, Kyoto University, Kyoto, Japan.

[2]Institute of Space and Astronautical Science, Sagamihara, Japan.

[3]Department of Science, Hokkaido University, Sapporo, Japan.

[4]Department of Information System, Osaka Institute of Technology, Hirakata, Japan.

[5]Radio Science Center for Space and Atmosphere, Kyoto University, Uji, Japan.

This preprint was prepared with AGU's LaTeX macros v5.01. File elfnoise-distrib formatted July 4, 2001.

Plate captions

Plate 1. (a-h) Dynamic spectra obtained by multichannel analyzer (MCA) and pitch angle sorted energy spectograms of electrons and ions obtained by low-energy particle detector (LEP).

Plate 2. (a-h) A summary plot of thermal and suprathermal ions observed by suprathermal ion mass spectrometer (SMS).

Plate 3. Dynamic spectra of an electric field obtained by wideband receiver (WBA) and the angle between the wire antenna and the geomagnetic field line.

Plate 4. Intensity of electric components of the broadband noise at 5 Hz.

Plate 5. (a-c) Local time dependence of the broadband noise at 5 Hz.

Plate 6. (a-c) Kp dependence of the broadband noise at 5 Hz.

Plate 7. Seasonal variation on the broadband noise. (a-d) The average intensity of the electric field at 5 Hz in the Northern Hemisphere. (e-h) The average intensity of the electric field at 5 Hz in the Southern Hemisphere.

Figure captions

Figure 1. Waveforms of intermittent noise observed by WBA.

Figure 2. Correlation between spectral density of broadband noise and energy density of heated ions. The circles and pluses mean that the data were obtained in the dayside and in the nightside, respectively.

Figure 3. Coverage of the Akebono orbits used for the statistical study.

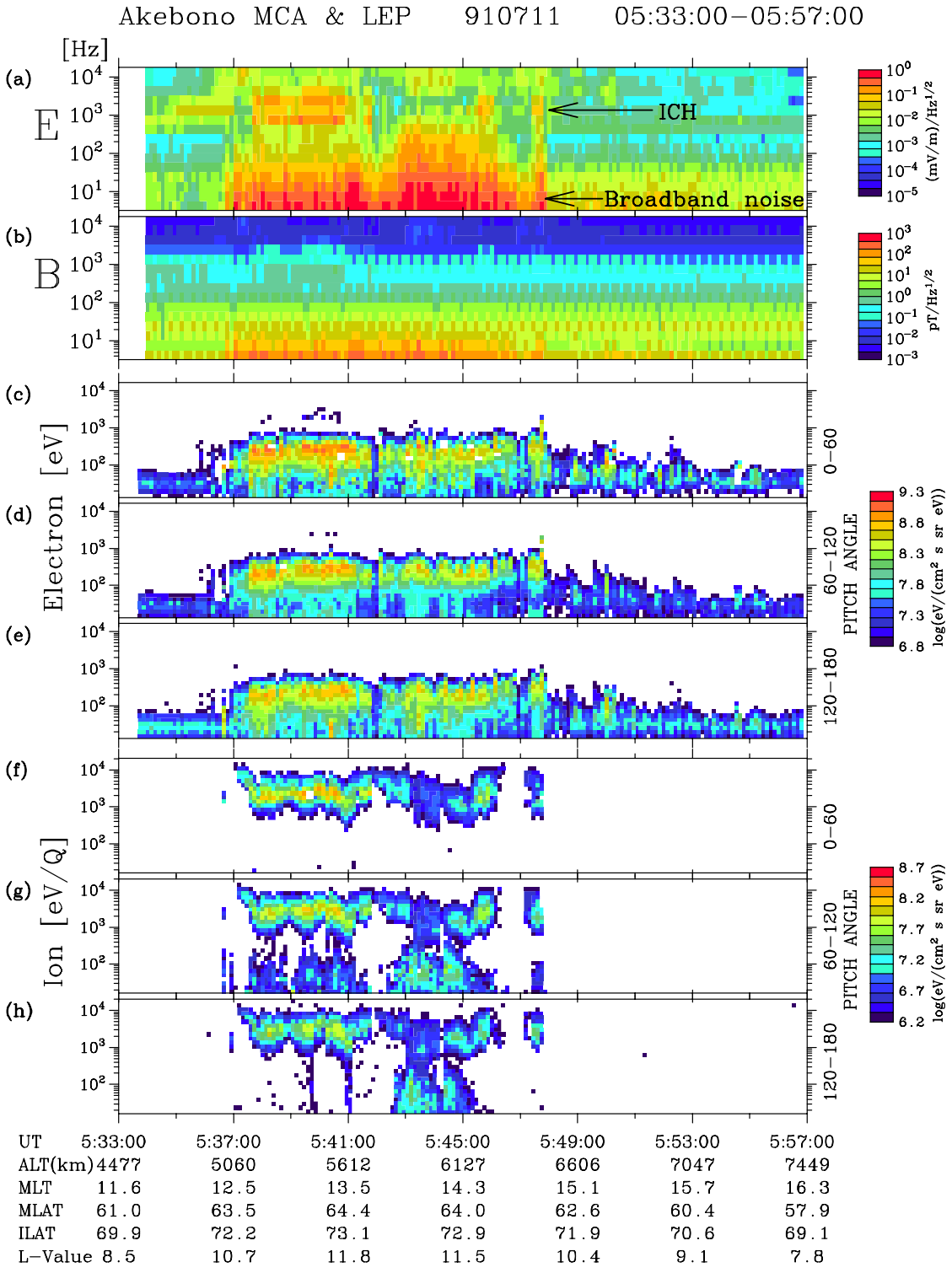
Akebono MCA & LEP 910711 05:33:00−05:57:00
[Hz]
(a)
E
ICH
Broadband noise
(mV/m)/Hz^1/2
(b)
B
pT/Hz^1/2
(c)
(d)
(e)
Electron [eV]
0−60
60−120
120−180
PITCH ANGLE
log(eV/(cm² s sr eV))
(f)
(g)
(h)
Ion [eV/Q]
UT 5:33:00 5:37:00 5:41:00 5:45:00 5:49:00 5:53:00 5:57:00
ALT(km) 4477 5060 5612 6127 6606 7047 7449
MLT 11.6 12.5 13.5 14.3 15.1 15.7 16.3
MLAT 61.0 63.5 64.4 64.0 62.6 60.4 57.9
ILAT 69.9 72.2 73.1 72.9 71.9 70.6 69.1
L−Value 8.5 10.7 11.8 11.5 10.4 9.1 7.8

Plate. 1

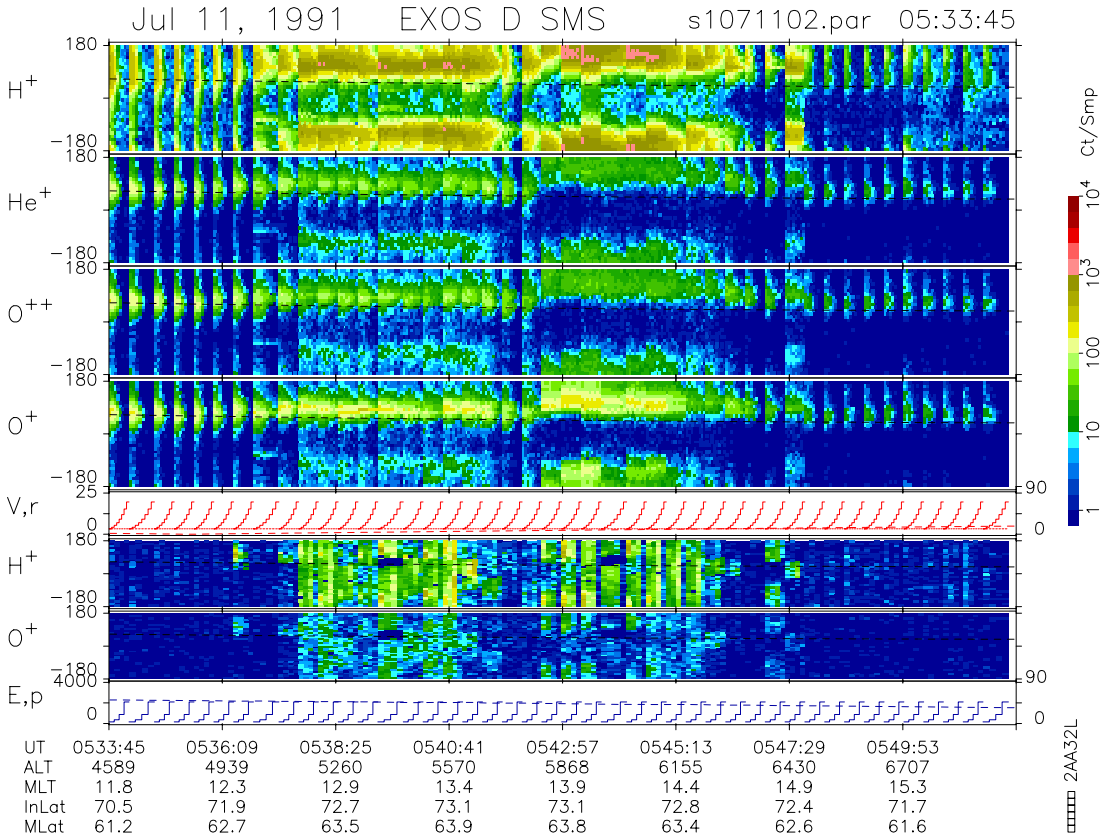
Jul 11, 1991 EXOS D SMS s1071102.par 05:33:45
H+
He+
O++
O+
V,r
H+
O+
E,p
180
−180
25
0
90
4000
Ct/Smp
10^4
10^3
100
10
1
2AA32L
UT 0533:45 0536:09 0538:25 0540:41 0542:57 0545:13 0547:29 0549:53
ALT 4589 4939 5260 5570 5868 6155 6430 6707
MLT 11.8 12.3 12.9 13.4 13.9 14.4 14.9 15.3
InLat 70.5 71.9 72.7 73.1 73.1 72.8 72.4 71.7
MLat 61.2 62.7 63.5 63.9 63.8 63.4 62.6 61.6

Plate. 2

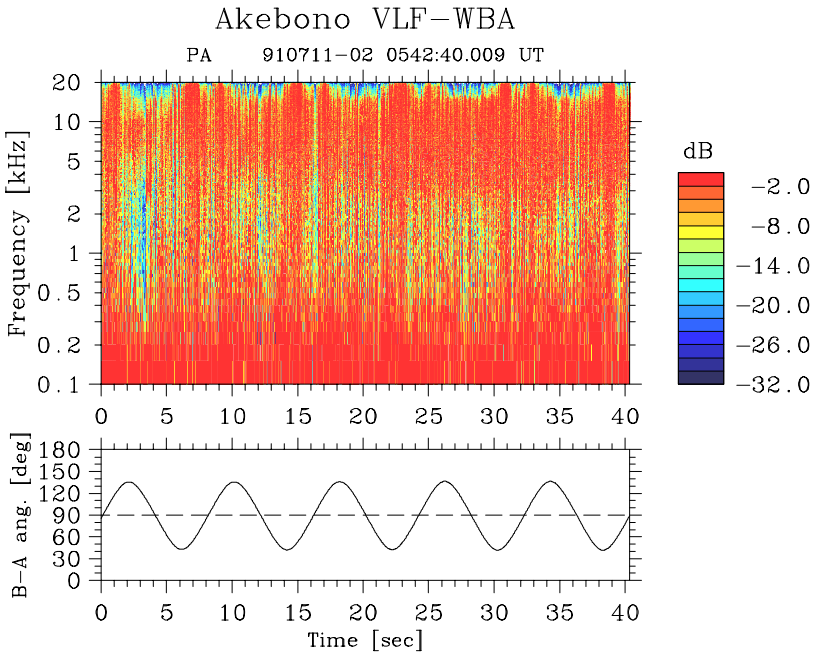
Akebono VLF−WBA
PA 910711−02 0542:40.009 UT
Frequency [kHz]
20
10
5
2
1
0.5
0.2
0.1
0 5 10 15 20 25 30 35 40
B−A ang. [deg]
180
150
120
90
60
30
0
0 5 10 15 20 25 30 35 40
Time [sec]
dB
−2.0
−8.0
−14.0
−20.0
−26.0
−32.0

Plate. 3

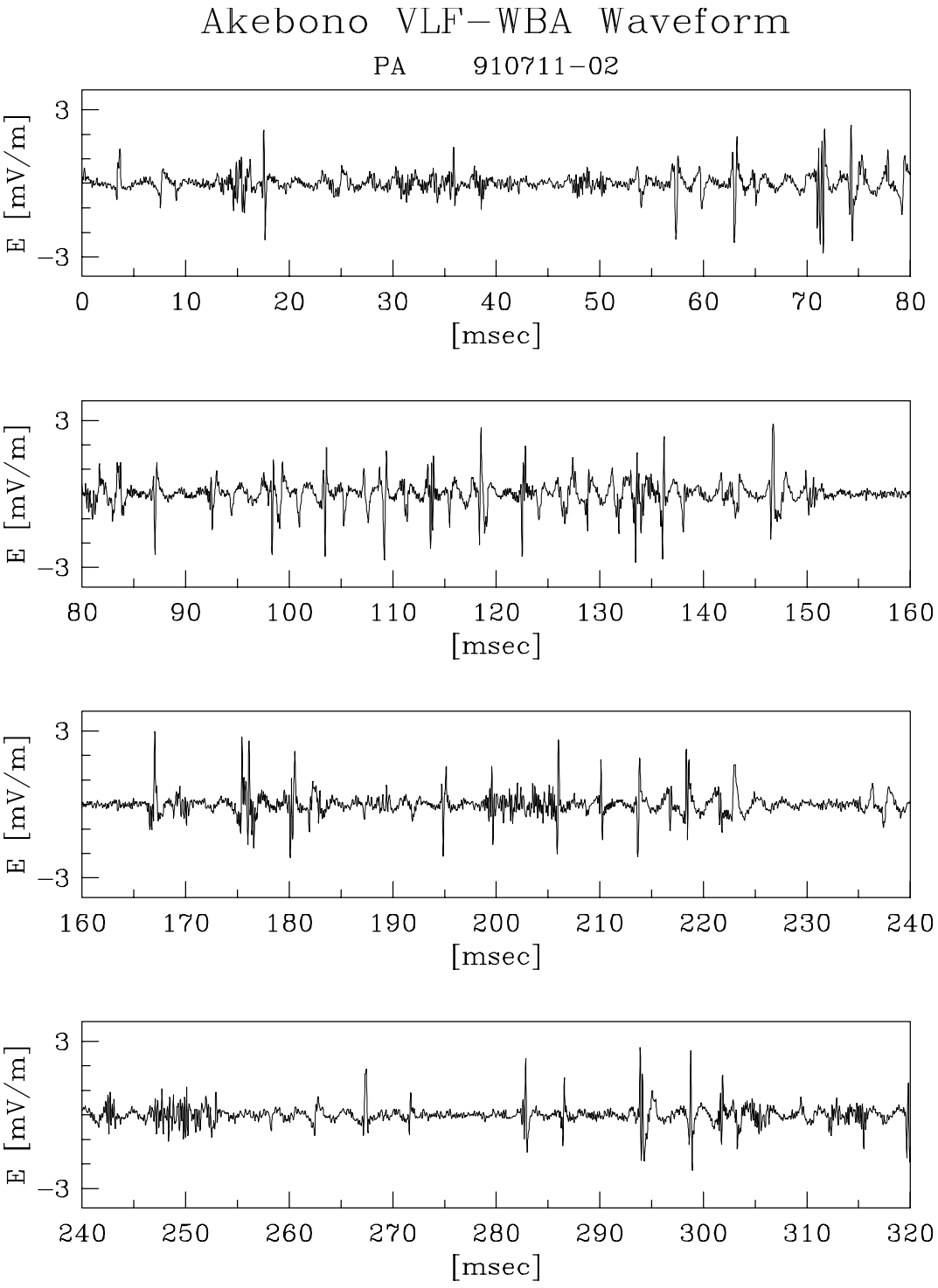
Akebono VLF−WBA Waveform
PA 910711−02
E [mV/m]
3
−3
0 10 20 30 40 50 60 70 80
[msec]
80 90 100 110 120 130 140 150 160
[msec]
160 170 180 190 200 210 220 230 240
[msec]
240 250 260 270 280 290 300 310 320
[msec]
05:42:44.929−05:42:45.248 UT

Figure. 1

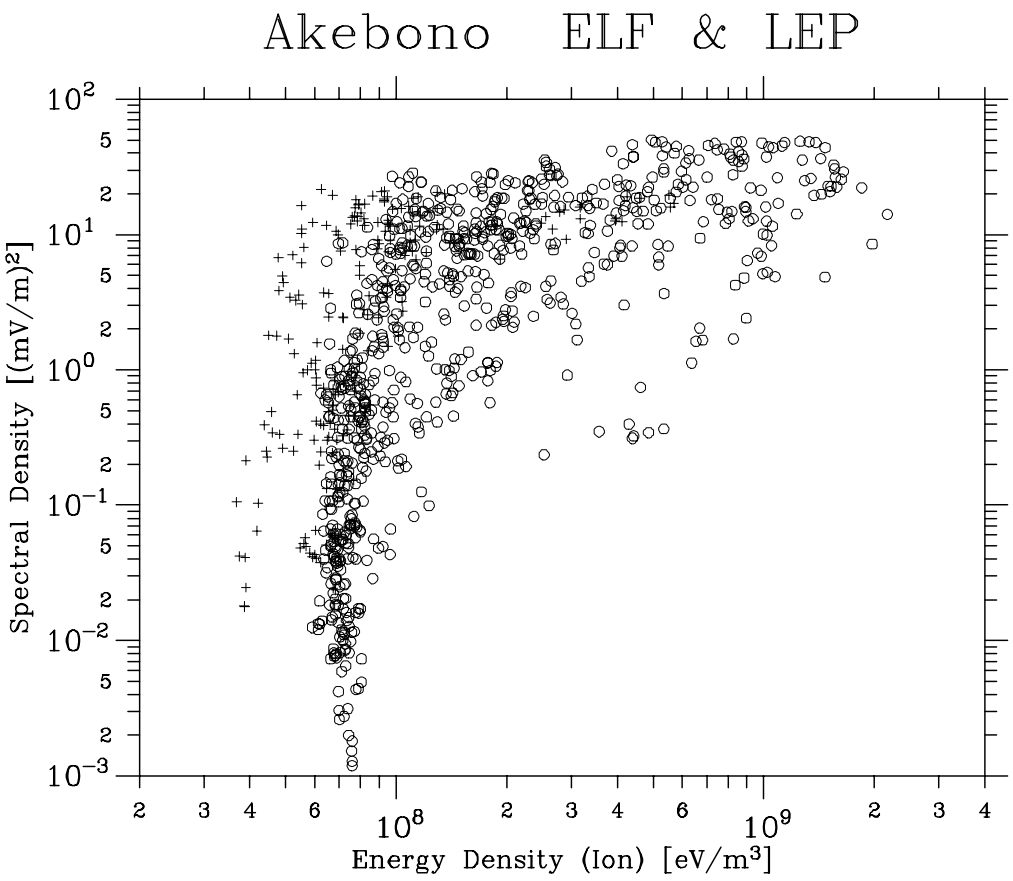
Akebono ELF & LEP
Spectral Density [(mV/m)²]
Energy Density (Ion) [eV/m³]

Figure. 2

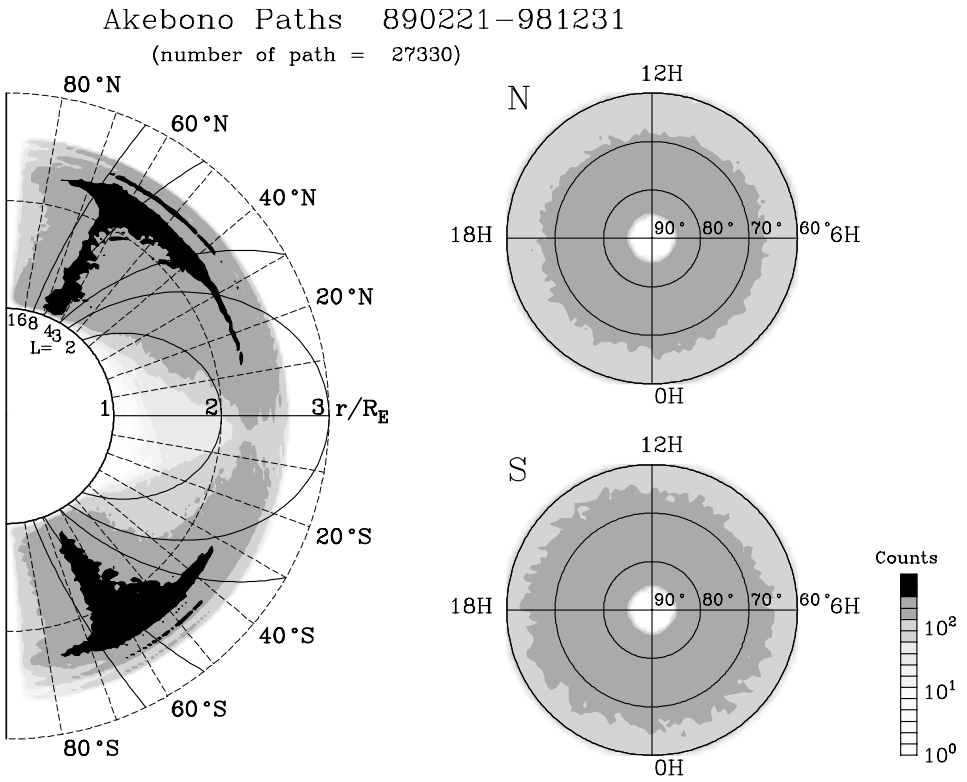
Akebono Paths 890221−981231
(number of path = 27330)
80°N
60°N
40°N
20°N
20°S
40°S
60°S
80°S
16 8 4 3 2
L=
1
2
3
r/R_E
N
12H
18H
6H
0H
90°
80°
70°
60°
S
Counts
10^2
10^1
10^0

Figure. 3

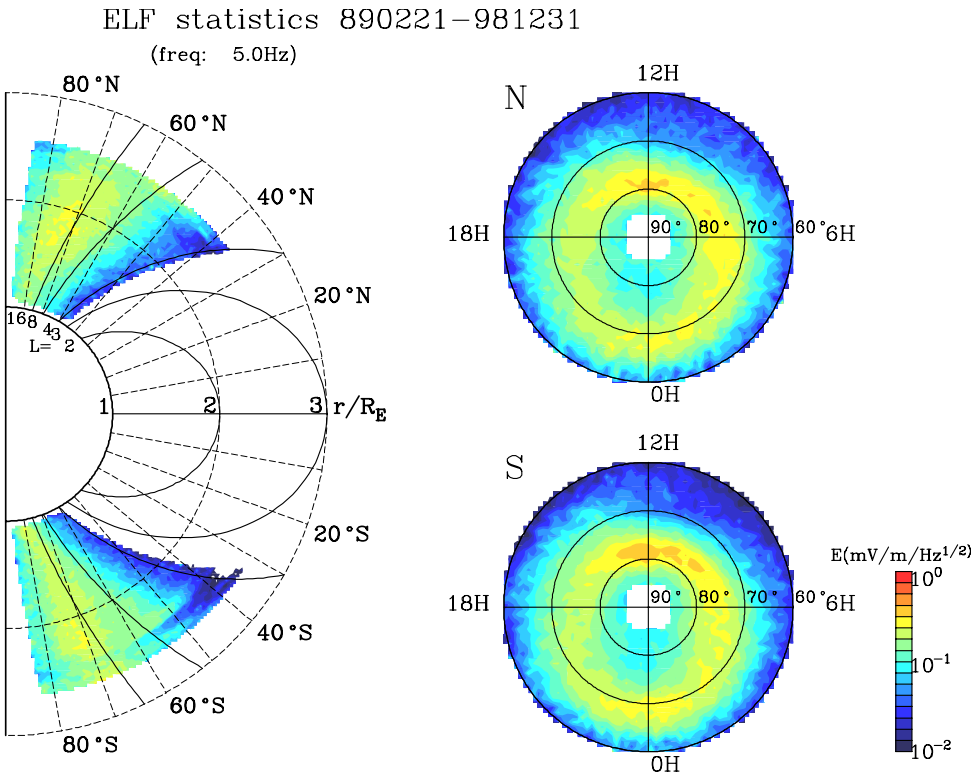
ELF statistics 890221−981231
(freq: 5.0Hz)
80°N
60°N
40°N
20°N
20°S
40°S
60°S
80°S
16 8 4 3 2
L=
1
2
3
r/R_E
N
S
12H
18H
6H
0H
90°
80°
70°
60°
E(mV/m/Hz^1/2)
10^0
10^-1
10^-2

Plate. 4

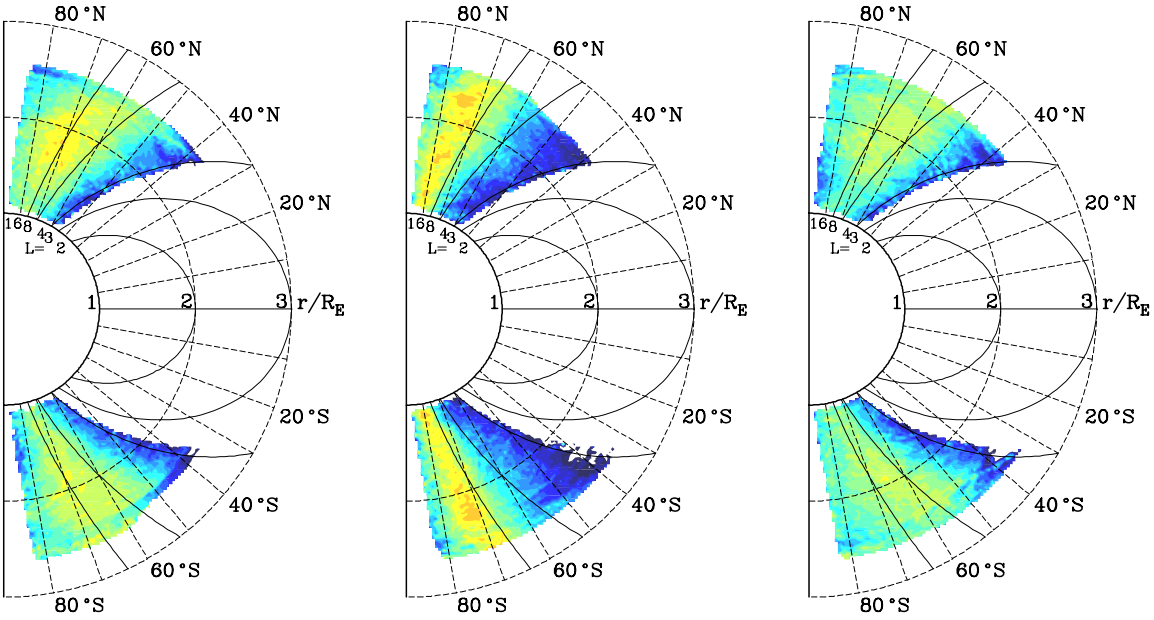

(a) $0 \leq \mathrm{MLT} \leq 8$ (b) $8 \leq \mathrm{MLT} \leq 16$ (c) $16 \leq \mathrm{MLT} \leq 0$

Plate. 5

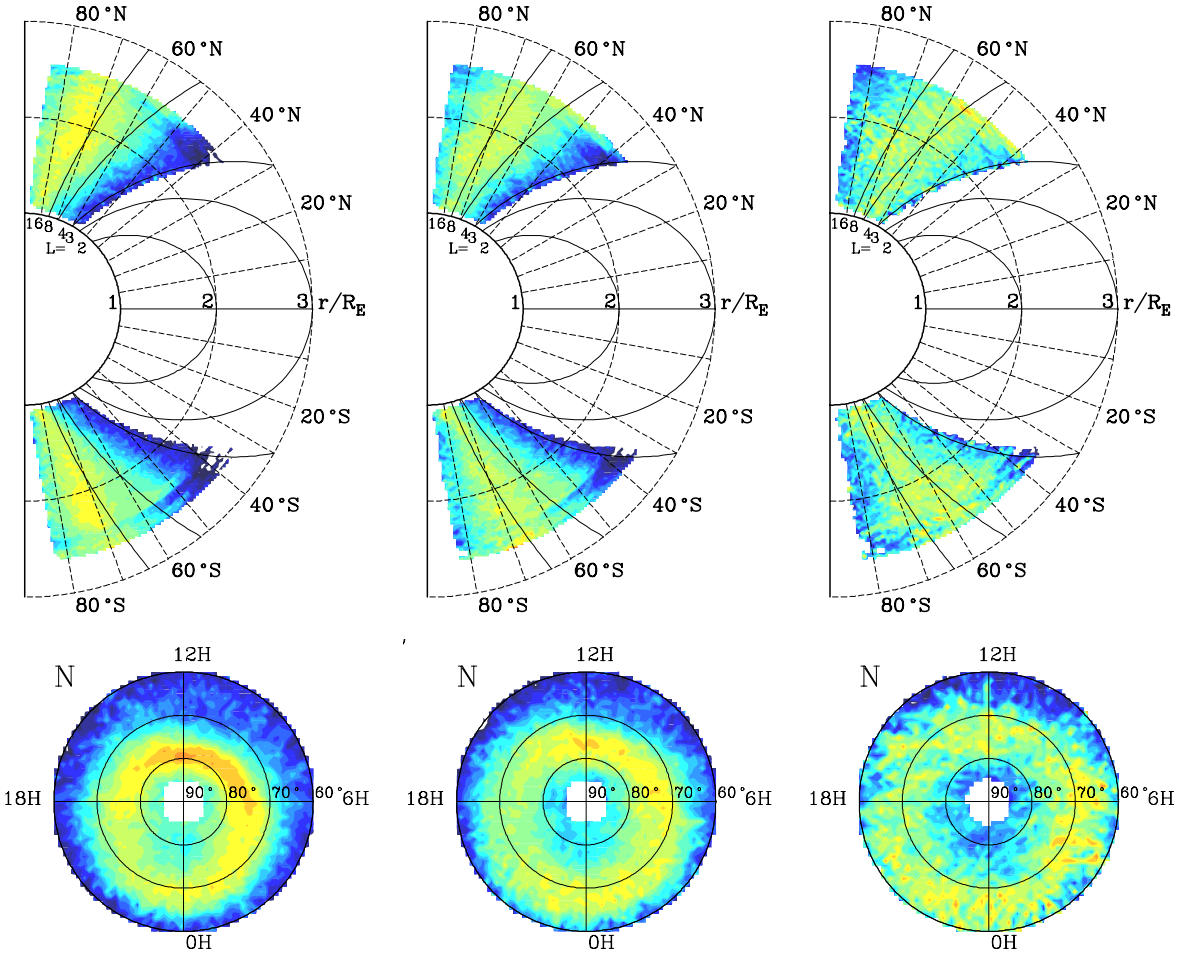

(a) $Kp \leq 2+$ (b) $3- \leq Kp \leq 4+$ (c) $5- \leq Kp$

Plate. 6

Northern Hemisphere

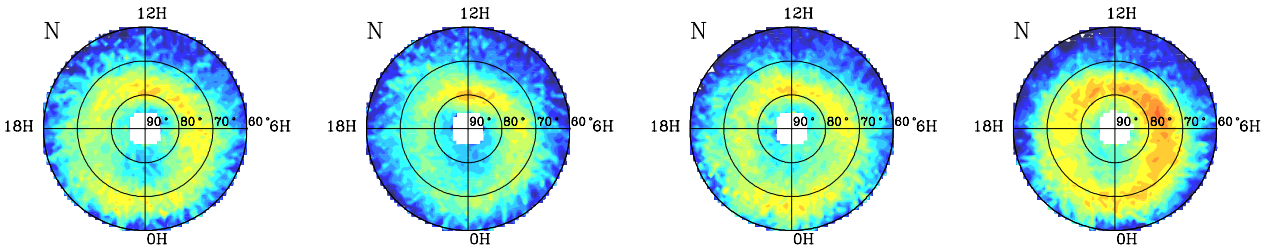

(a) (b) (c) (d)

Southern Hemisphere

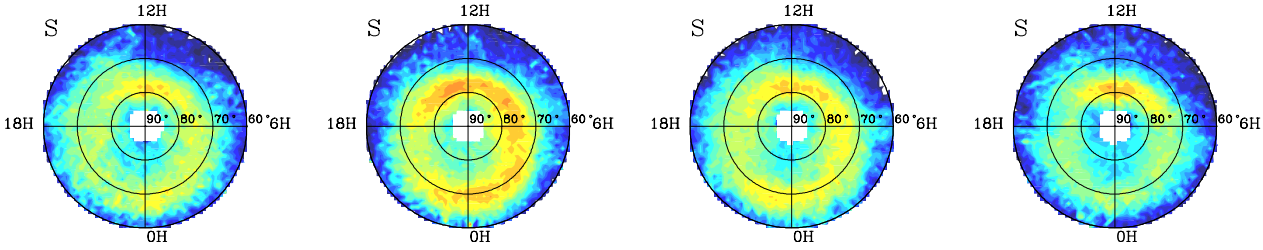

(e) (f) (g) (h)

Feb. 7 – May 6 | May 7 – Aug. 6 | Aug. 7 – Nov. 6 | Nov. 7 – Feb. 6

Plate. 7